Crystallographically resolved damage initiation in advanced high strength steel

Shakerifard, B.; Galan Lopez, J.; Hisker, F.; Kestens, L. A.I.

Crystallographically resolved damage initiation in advanced high strength steel

To cite this article: B. Shakerifard *et al* 2018 *IOP Conf. Ser.: Mater. Sci. Eng.* **375** 012022

View the article online for updates and enhancements.

Related content

- Research and Development of the Advanced High Strength Steel for the Mining Machinery
  Linhao Gu, Jianming Liu, Shiping Lu et al.

- Experimental Study on Failure Mechanism of Advanced High Strength Steels in Air Bending Process
  N Pornputsiri and K Kanlayasiri

- Research on the Application of High Strength Steel for 750kV Combined Framework
  Hongtao Ju, Wen Jiang, Li Yang et al.

Crystallographically resolved damage initiation in advanced high strength steel

B. Shakerifard[1], J. Galan Lopez[2], F. Hisker[3] and L. A. I. Kestens[1,4]

[1] Delft University of Technology, Delft, The Netherlands.
[2] M2i, Materials Innovation Institute, Delft, The Netherlands.
[3] ThyssenKrupp Steel Europe AG, Duisburg, Germany.
[4] Ghent University, Ghent, Belgium.

b.shakerifard@tudelft.nl

Abstract. Recently, the third generation of advanced high strength steels (AHSSs) show promising properties for automotive applications. The improvement of macroscopic mechanical performance is not feasible without a deep understanding of the micromechanical behavior and failure micro-mechanisms involved during its response under various loading conditions. In this study, a uniaxial tensile test is conducted on a low silicon bainitic steel with second phase constituents (martensite and carbides). A comprehensive image processing on SEM micrographs is performed in order to quantify the damage evolution as a function of plastic deformation. A new methodology is examined to address the correlation between crystallographic orientation and damage initiation. In this multiphase steel, it appears that orientation dependence of damage initiation is blurred by the presence of different phases and hence there is not an obvious preferential orientation from where damage has initiated.

1. Introduction

In multiphase steels, it has been well studied that microstructural heterogeneities such as different phases with various mechanical contrast, play a significant role in the partitioning of stress (and/or strain) during plastic deformation [1-4]. Hence, at the microstructure level, these local deformation incompatibilities may induce void formation in order to dissipate the plastic work.

The morphological effect (size, shape and distribution) of the second phase (*i.e* martensite) on ductile damage initiation in dual phase steels has been extensively studied by advanced experiments and crystal plasticity models [5-8]. In addition, the role of crystallographic orientation in stress (and/or strain) partitioning is another factor that needs to be considered. Jia *et al* have shown in a duplex stainless steel that at high macroscopic stresses when all grains in both constituent phases deform plastically, the role of the crystallographic orientation anisotropy on stress-strain partitioning is more significant than the phase contrast stresses [9]. The role of crystallographic orientation on damage initiation at relatively high levels of plastic deformations was also observed on metal-matrix [10] and rigid fiber composites [11] or alternatively in an austenitic stainless steel under the cyclic loading condition [12]. Eventually, the competing effect of phase contrast, with various topologies, and crystallographic orientation on damage initiation is a frequent topic of investigation [6, 12, 13].

In the current work, first a complete quantitative analysis on distribution of voids and its correlation to the strain is performed. This allows deriving a criterion for the initiation of the damage within the microstructure. In order to study the role of crystallographic orientation on damage initiation, an electron backscatter diffraction (EBSD) based analysis is used to capture the orientations around the voids. Afterwards, textures are compared in order to understand the correlation between damage and crystallographic orientation.

2. Methodology

2.1. Material
The bainitic seel used in the current study is a low silicon bainitic steel. The chemical composition is shown in table 1. The 1 mm thick sheet of cold rolled ferritic-pearlitic steel is annealed above the Ac3 temperature and quenched to the bainite holding temperature for a particular holding time, which results in a microstructure that is composed of a predominant bainite phase and a small fraction of martensite (~3%). Following, bainite transformation, the material is quenched to room temperature.

Table 1. Chemical composition of the studied bainitic steel (wt.%).

Elements	C%	Mn%	Si%	Cr%	Al%	P%	S%	N%
Bainitic steel	0.215	1.96	0.10	0.61	0.020	0.007	0.0027	0.005

2.2. Mechanical test
Two uniaxial tensile tests were conducted at room temperature with strain rates of 6.10^{-3} and 8.10^{-1} s^{-1} in elastic and plastic regions of flow curve, respectively. The tensile tests were carried out according to the DIN EN 6892-1 standard using a Zwick Z100 tensile machine. The flat specimens with gauge length of 25 mm are loaded along the rolling direction (RD). Two interrupted tensile tests were performed in the uniform and non-uniform regions of the plastic domain in order to capture the evolution of the voids within the microstructure.

2.3. Microstructure characterization
Specimen surfaces are prepared by the conventional metallographic procedure of grinding, diamond polishing and eventually polishing with colloidal SiO2. A scanning electron microscope FEI® (Quanta FEG 450) equipped with EBSD detector is used to characterize the microstructure of the samples prior to and after the tensile test. EBSD measurements are carried out with the step size of 0.05 μm in the conventional configuration of 70° inclined samples. Results obtained from EBSD analysis are post processed in the EDAX-OIM Analysis^{TM} software.

In order to quantify the area fraction and number density of voids within the microstructure after the tensile test, a high resolution FEG-SEM (FEI XL30) was used. An area of approximately $1x1$ mm^2 was scanned by running an image acquisition script to automatically capture 1000 secondary electron SEM micrographs. The contiguous collection of micrographs with pixel size of 31 nm could enable to detect all the micro-voids within the microstructure. Eventually, all the images were merged and processed to quantify voids by image processing using Matlab$^@$ software. A void size criterion was considered in which all the voids larger than $0.1 μm^2$ ($\approx$33 pixels) were counted.

3. Results and discussions

3.1. Mechanical response
The mechanical response of the material is shown in figure 1. Considering the engineering flow curve of the material, small non-uniform region is observed. Therefore, the material could not accommodate considerable plastic deformation right after the uniform region of the flow curve. The localized necking behaviour of the material also confirms the small post-necking region of the flow curve.
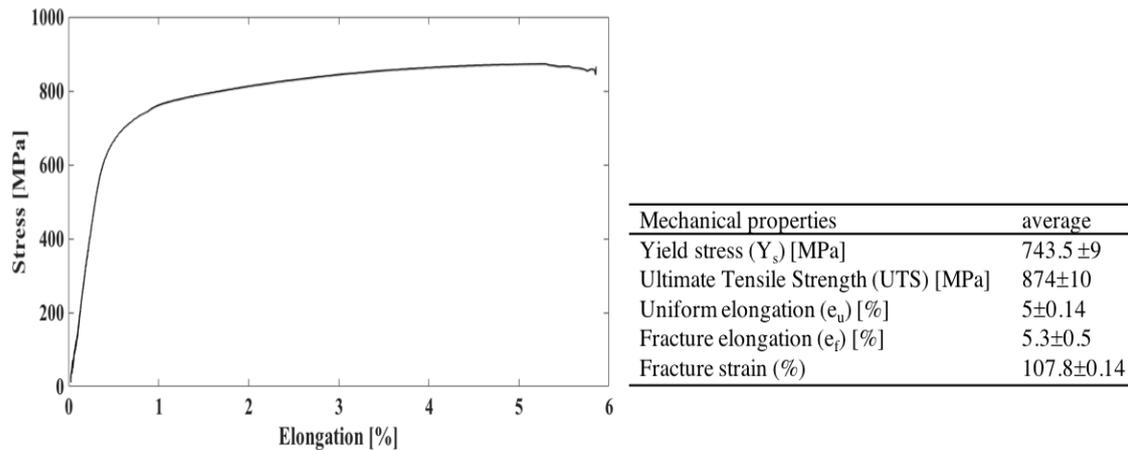
Mechanical properties	average
Yield stress (Y_s) [MPa]	743.5 ±9
Ultimate Tensile Strength (UTS) [MPa]	874±10
Uniform elongation (e_u) [%]	5±0.14
Fracture elongation (e_f) [%]	5.3±0.5
Fracture strain (%)	107.8±0.14

Figure 1. Engineering flow curve of the material under quasi-static loading condition.
Mechanical properties calculated from the tensile curve.

3.2. Microstructure characterization

3.2.1. Void mapping. The void map shown in figure 2(a), reveals the accumulation of voids adjacent to the fracture surface. Voids are only initiated after uniform plastic deformation at the finishing stage of necking, prior to final failure of the material. Indeed, the interrupted tensile sample at the elongation of 5% confirmed the absence of void formation within the microstructure prior to necking. However, in dual phase (DP) ferritic and martensitic steels, it has been observed that voids started to nucleate at earlier stages of plastic deformation [14]. The retardation of the void initiation in this bainitic steel is a consequence of the less mechanical phase contrast between bainite and martensite compared to ferrite and martensite phases in DP steels [15].

The voids are quantified by two parameters: the void number density and the void area fraction. The void number density is related to void nucleation activity within the microstructure during deformation. The void area fraction reveals information with regard to subsequent steps of the micro-mechanisms of ductile damage initiation, growth and coalescence (see figure 2b). True plastic strain values are calculated in equally distanced intervals from the fracture surface based on the transversal and normal strains. The strain gradient, as function of distance from the fracture surface, is remarkably high close to the fracture surface. It is observed that both factors increase with plastic deformation. These two parameters are relatively low until almost 72% of plastic deformation. However, upon reaching this strain level, a pronounced increase in the damage incidents is observed. The localization of the deformation (localized necking) close to fracture surface leads to higher triaxiality of the stress mode and, consequently, damage is accumulated in this region.

3.2.2. Correlation between crystallographic orientation and damage. The role of crystallographic orientation on damage initiation was investigated. Scanning electron micrographs of the etched microstructure showed that damage has occurred at the interface of bainite and martensite (B/M). This reveals the presence of mechanical phase contrast between B and M, which causes stress (and/or strain) partitioning. This incompatibility at some critical moment when the imposed loads cannot be relaxed anymore by plastic glide, leads to interface tearing or void initiation. In addition, the role of crystallographic orientation on strain (and/or stress) partitioning is inevitable. In this effort, 33 voids

have been studied locally by EBSD in order to capture the local surrounding orientations. The selection procedure is schematically represented in figure 3. As it is shown in figure 3b, an area with sides of approximately 3 times the void diameter was considered as the local environment surrounding a specific void.

Due to severe plastic deformation and distortion in the crystal lattices in the vicinity of the voids, a poor pattern quality was observed. Only orientations with confidence index above 0.1 were retained. Later, the ODF was derived from approximately 131,000 void neighbouring pixels, represented in the $\varphi_2 = 45°$ section of Euler space and denominated the VODF (Void ODF), cf. Fig. 4b. Because on the level of individual voids sample symmetry has to be ignored and thus the Euler space limits are set to $0 < \varphi_1 < 360°$ and $0 < \varphi_2, \Phi < 90$. Similarly, also the texture was considered of the regions with no voids, which produces the No-Void ODF (NVODF), cf. Figure 4c. It is expected that regions with no voids have more dispersed orientations compared to regions selected around the voids. Therefore, after merging all of these orientations away from the voids, the No-Void ODF (NVODF) plot reveals smoother distribution.

As it was mentioned earlier in section 3.2.1, during uniform plastic deformation no microstructural damage has appeared, thus, the deformation texture of the material at the UTS point, cf. Figure 4a, can be considered as a reference texture from which voids will be initiated. By merging the textures from the void neighbouring grains and the grains away from the voids, the entire texture of the necked region is obtained, i.e. the Neck-ODF, cf. Figure 4d. This study is a post-mortem analysis, which implies that all orientations regarding VODF and NVODF were captured after final failure. Moreover, it is not clear which interface was the origin of the damage initiation spot. The rectangular region of interest around the voids includes all possible orientations from which the voids might have initiated.
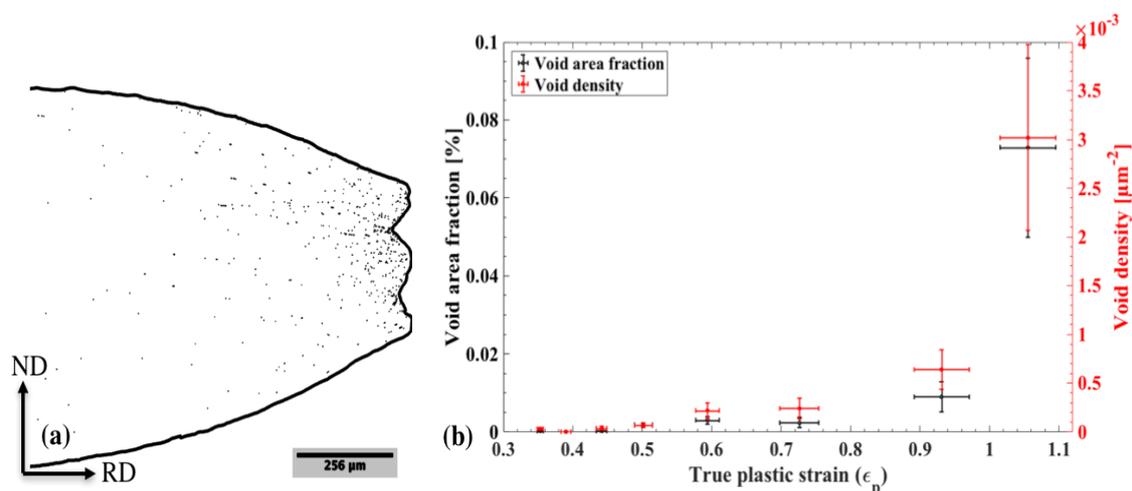

Figure 2. Void mapping analysis: (a) distribution of voids within the microstructure (in order to enhance the visual contrast between voids and the background matrix, voids are enlarged approximately 100x) and (b) void area fraction and void density as a function of true plastic strain.
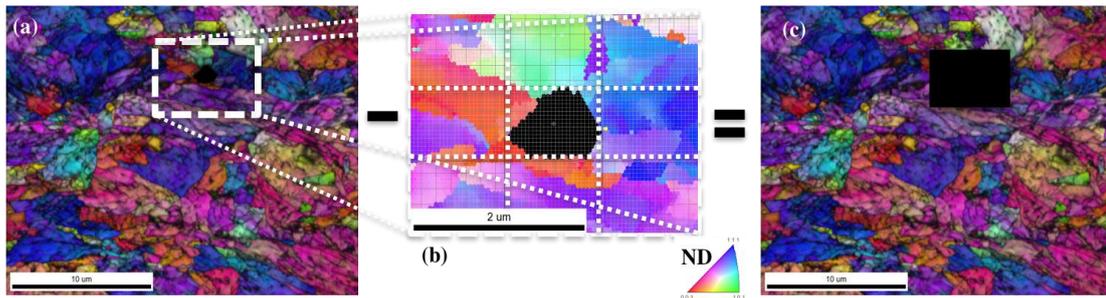
Figure 3. Schematic illustration of orientation selection on an overlapped image quality and inverse pole figure map; (a) complete area of analysis, (b) area selected around the void with faces approximately equal to 3 times of a void diameter and (c) remaining area.

Figure 4 shows the textures in the $\varphi_2=45°$ section of the material at two different strain levels, uniform and post uniform, respectively. By visually comparing the VODF and NVODF with respect to the Neck-ODF it is observed that the NVODF closer resembles the texture observed in the necked region (Neck-ODF). Conversely, by visually comparing VODF and NVODF with the uniform texture, it appears that the VODF better resembles the uniform ODF. This can be explained by the fact that the local stress relaxation process at a certain moment is occurring by the void initiation rather than by plastic deformation accommodated by dislocation glide. Upon further macroscopic deformation, two
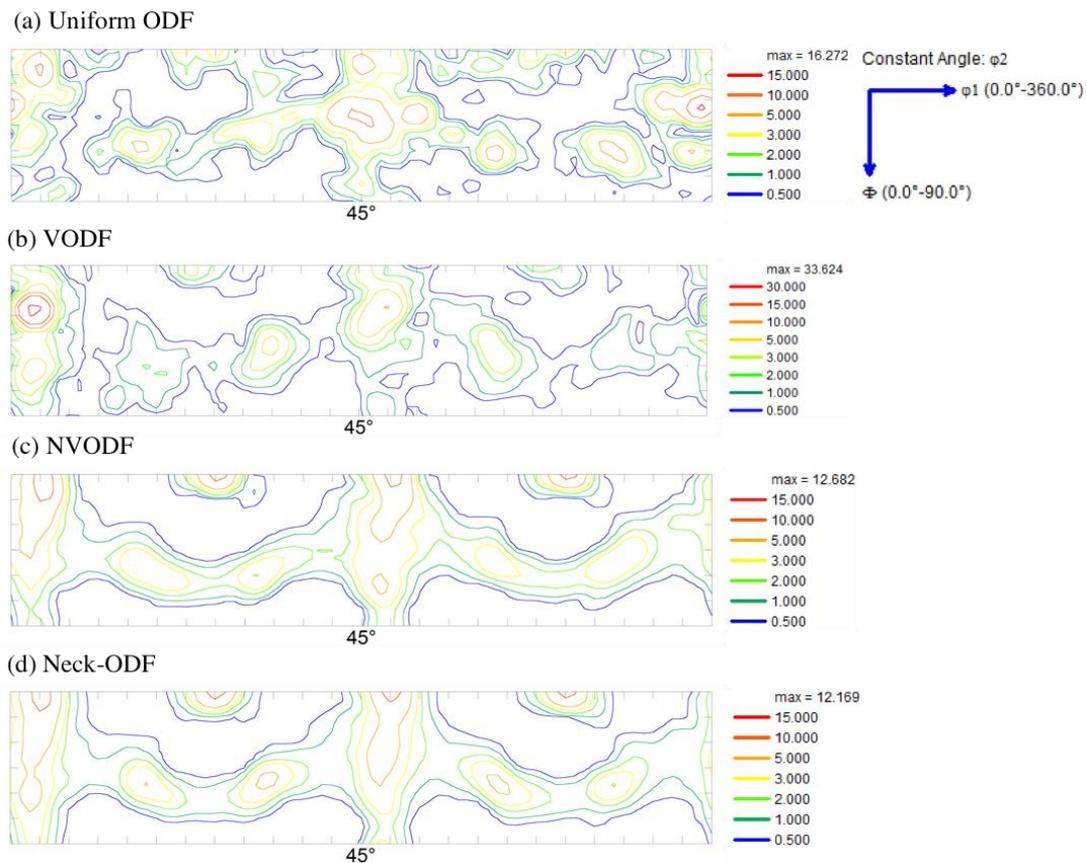

Figure 4. $\varphi_2=45°$ section of ODFs of the material at two different deformation levels; (a) Uniform deformation UODF (calculated from 796000 data points), (b) post uniform VODF (131000 data points), (c) post uniform NVODF (460000 data points) and (d) Necking or post uniform ODF consist of the merged ODFs in b and c.

micro mechanisms can dissipate the local stress concentration produced by the presence of a void, i.e. void growth and/or local further plasticity surrounding the initiated void. The results from the comparison between UODF, VODF and Neck-ODF demonstrate that after voids were formed, the local stress dissipation process around voids is rather governed by void growth than local plasticity as the Void-ODF clearly resembles the uniform ODF. Nevertheless, a void is nothing but a free surface within the microstructure, which may relax the local constraint of the surrounding grains and thus can potentially ease the local plastic deformation. However, the competing role of the locally hardening and free surface lead to the final contribution of plasticity and/or void growth on the stress relaxation.

3.3. Conclusion

Two characterization methods were used to study the initiation of damage within the microstructure of low silicon bainitic steel. It was found that damage initiation and extent of damage could be accurately characterized by void mapping. It was observed that voids are only initiated at terminal stage of deformation prior to final fracture. At approximately 55% of true plastic strain, voids start to initiate.
A new methodology was examined to address the role of crystallographic orientation on damage initiation. In the necked region of the sample, the microstructure was divided in two parts: (i) the crystallographic orientations of the grains surrounding 33 voids were selected and represented by the Void-ODF, (ii) whereas the regions away from the voids represented the no voids ODF (NVODF). It was observed that the VODF more resembles the texture of the uniformly deformed region, outside the necked region. The post mortem crystallographic orientation analysis around voids revealed that after void initiation, the local stress relaxation process is rather controlled by void growth than by further local plastic deformation.

References

1. Ahmad, E., et al., *Effect of microvoid formation on the tensile properties of dual-phase steel.* Journal of Materials Engineering and Performance, 2000. **9**(3): p. 306-310.
2. Avramovic-Cingara, G., et al., *Effect of martensite distribution on damage behaviour in DP600 dual phase steels.* Materials Science and Engineering a-Structural Materials Properties Microstructure and Processing, 2009. **516**(1-2): p. 7-16.
3. He, X.J., N. Terao, and A. Berghezan, *Influence of Martensite Morphology and Its Dispersion on Mechanical-Properties and Fracture Mechanisms of Fe-Mn-C Dual Phase Steels.* Metal Science, 1984. **18**(7): p. 367-373.
4. Steinbrunner, D.L., D.K. Matlock, and G. Krauss, *Void Formation during Tensile Testing of Dual Phase Steels.* Metallurgical Transactions a-Physical Metallurgy and Materials Science, 1988. **19**(3): p. 579-589.
5. Tasan, C.C., et al., *Integrated experimental-simulation analysis of stress and strain partitioning in multiphase alloys.* Acta Materialia, 2014. **81**: p. 386-400.
6. Tasan, C.C., et al., *Strain localization and damage in dual phase steels investigated by coupled in-situ deformation experiments and crystal plasticity simulations.* International Journal of Plasticity, 2014. **63**: p. 198-210.
7. Tasan, C.C., J.P.M. Hoefnagels, and M.G.D. Geers, *Identification of the continuum damage parameter: An experimental challenge in modeling damage evolution.* Acta Materialia, 2012. **60**(8): p. 3581-3589.
8. Yan, D.S., C.C. Tasan, and D. Raabe, *High resolution in situ mapping of microstrain and microstructure evolution reveals damage resistance criteria in dual phase steels.* Acta Materialia, 2015. **96**: p. 399-409.
9. Jia, N., et al., *Interactions between the phase stress and the grain-orientation-dependent stress in duplex stainless steel during deformation.* Acta Materialia, 2006. **54**(15): p. 3907-3916.

10.	Needleman, A. and V. Tvergaard, *Comparison of Crystal Plasticity and Isotropic Hardening Predictions for Metal-Matrix Composites.* Journal of Applied Mechanics-Transactions of the Asme, 1993. **60**(1): p. 70-76.

11.	Nugent, E.E., R.B. Calhoun, and A. Mortensen, *Experimental investigation of stress and strain fields in a ductile matrix surrounding an elastic inclusion.* Acta Materialia, 2000. **48**(7): p. 1451-1467.

12.	Li, R.G., et al., *Unraveling submicron-scale mechanical heterogeneity by three-dimensional X-ray microdiffraction.* Proceedings of the National Academy of Sciences of the United States of America, 2018. **115**(3): p. 483-488.

13.	de Geus, T.W.J., et al., *Microscopic plasticity and damage in two-phase steels: On the competing role of crystallography and phase contrast.* Mechanics of Materials, 2016. **101**: p. 147-159.

14.	Han, S.K. and H. Margolin, *Void Formation, Void Growth and Tensile Fracture of Plain Carbon-Steel and a Dual-Phase Steel.* Materials Science and Engineering a-Structural Materials Properties Microstructure and Processing, 1989. **112**: p. 133-141.

15.	de Geus, T.W.J., R.H.J. Peerlings, and M.G.D. Geers, *Microstructural topology effects on the onset of ductile failure in multi-phase materials - A systematic computational approach.* International Journal of Solids and Structures, 2015. **67-68**: p. 326-339.